Article

Cell Reports

Wolf-Hirschhorn Syndrome Candidate 1 Is Necessary for Correct Hematopoietic and B Cell Development

Graphical Abstract

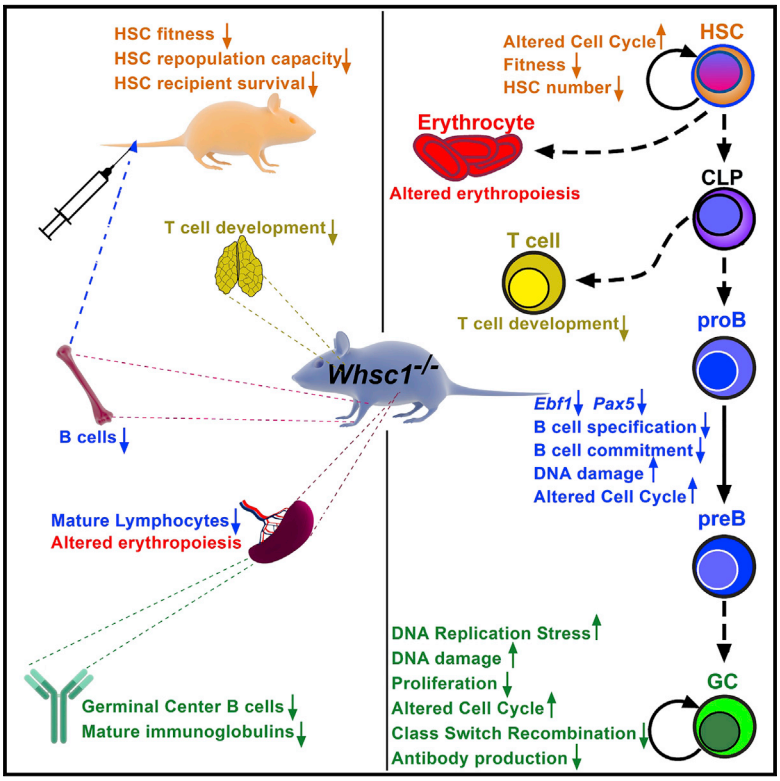

Highlights

- Hemizygous loss of *Whsc1* causes a progressive decline of lymphocyte numbers with age
- *Whsc1* deficiency reduces hematopoietic stem cell fitness and repopulation capacity
- *Whsc1*$^{-/-}$ B cell precursors have defective B cell lineage specification and commitment
- *Whsc1*$^{-/-}$ GC cells present impaired CSR, altered cell cycle, and DNA replicative stress

Authors

Elena Campos-Sanchez, Nerea Deleyto-Seldas, Veronica Dominguez, ..., Jane A. Skok, Maria Luisa Martinez-Frias, Cesar Cobaleda

Correspondence

cesar.cobaleda@csic.es

In Brief

Campos-Sanchez et al. show that *Whsc1* plays an important function in hematopoiesis in vivo, demonstrating a role for *Whsc1* in the immunodeficiency in Wolf-Hirschhorn syndrome. *Whsc1*-deficient blood cells are impaired at several developmental stages due to defects in hematopoietic stem cell fitness and B cell lineage specification and commitment, among other problems.

Accession Numbers

GSE84878
GSE88970

Campos-Sanchez et al., 2017, Cell Reports *19*, 1586–1601
May 23, 2017
http://dx.doi.org/10.1016/j.celrep.2017.04.069

OPEN ACCESS
CellPress

Cell Reports
Article

Wolf-Hirschhorn Syndrome Candidate 1 Is Necessary for Correct Hematopoietic and B Cell Development

Elena Campos-Sanchez,[1] Nerea Deleyto-Seldas,[1,12] Veronica Dominguez,[2] Enrique Carrillo-de-Santa-Pau,[3] Kiyoe Ura,[4] Pedro P. Rocha,[5] JungHyun Kim,[5] Arafat Aljoufi,[5] Anna Esteve-Codina,[6,7] Marc Dabad,[6,7] Marta Gut,[6,7] Holger Heyn,[6,7] Yasufumi Kaneda,[8] Keisuke Nimura,[8] Jane A. Skok,[5] Maria Luisa Martinez-Frias,[9,10,11] and Cesar Cobaleda[1,13,*]

[1]Department of Cell Biology and Immunology, Centro de Biologia Molecular Severo Ochoa (CBMSO), CSIC/UAM, Madrid 28049, Spain
[2]Transgenesis Service CNB-CBMSO CSIC/UAM, Madrid 28049, Spain
[3]Epithelial Carcinogenesis Group, Cancer Cell Biology Programme, Spanish National Cancer Research Centre (CNIO), Madrid 28029, Spain
[4]Department of Biology, Graduate School of Science, Chiba University, Yayoicho, Inage-ku, Chiba 263-8522, Japan
[5]Department of Pathology, New York University School of Medicine, New York, NY 10016, USA
[6]CNAG-CRG, Centre for Genomic Regulation (CRG), Barcelona Institute of Science and Technology (BIST), Barcelona 08028, Spain
[7]Universitat Pompeu Fabra (UPF), Barcelona 08002, Spain
[8]Division of Gene Therapy Science, Graduate School of Medicine, Osaka University, Yamada-oka, Suita, Osaka 565-0871, Japan
[9]ECEMC (Spanish Collaborative Study of Congenital Malformations), Madrid 28029, Spain
[10]CIAC (Research Center on Congenital Anomalies), Institute of Health Carlos III (ISCIII), Madrid 28029, Spain
[11]CIBER de Enfermedades Raras (CIBERER), U724, Madrid 28029, Spain
[12]Present address: Metabolism and Cell Signaling Group, CNIO, Madrid 28029, Spain
[13]Lead Contact
*Correspondence: cesar.cobaleda@csic.es
http://dx.doi.org/10.1016/j.celrep.2017.04.069

SUMMARY

Immunodeficiency is one of the most important causes of mortality associated with Wolf-Hirschhorn syndrome (WHS), a severe rare disease originated by a deletion in chromosome 4p. The WHS candidate 1 (*WHSC1*) gene has been proposed as one of the main genes responsible for many of the alterations in WHS, but its mechanism of action is still unknown. Here, we present in vivo genetic evidence showing that Whsc1 plays an important role at several points of hematopoietic development. Particularly, our results demonstrate that both differentiation and function of *Whsc1*-deficient B cells are impaired at several key developmental stages due to profound molecular defects affecting B cell lineage specification, commitment, fitness, and proliferation, demonstrating a causal role for WHSC1 in the immunodeficiency of WHS patients.

INTRODUCTION

Rare diseases affecting development, beyond their medical importance, offer us a unique opportunity to identify key genes involved in development and pathology. Wolf-Hirschhorn syndrome (WHS) is caused by the heterozygous loss of material in chromosome 4p arm (Battaglia et al., 2011, 2015). Patients suffer from serious problems, including immunodeficiency, seizures, developmental delay, and mental retardation. The increased susceptibility to infections is a major cause of morbidity and mortality among WHS patients (Hanley-Lopez et al., 1998). The heterozygous loss of the *Wolf-Hirschhorn Syndrome candidate 1* gene (*WHSC1*, also known as *MMSET* and *NSD2*) has been postulated to be the main responsible for the malformations and the immune deficiencies (Bergemann et al., 2005). *WHSC1* is also involved in other pathologies affecting B lymphocytes, like multiple myeloma (Chesi et al., 1998; Stec et al., 1998) and childhood B cell acute lymphoblastic leukemias (Huether et al., 2014; Jaffe et al., 2013). Furthermore, it belongs to the protein family of nuclear SET (Su(var)3-9, Enhancer-of-zeste, Trithorax) domain (NSD) proteins, whose other members are also involved in developmental and tumoral pathologies (Morishita and di Luccio, 2011). The WHSC1 protein contains a SET domain that confers it with histone-methyltransferase activity (Marango et al., 2008; Stec et al., 1998). Its most important in vivo activity is to mediate H3K36 mono- and di-methylation (Kuo et al., 2011), therefore acting as an epigenetic regulator (Kuo et al., 2011). Methylation at H3K36 has been associated with regulation of transcription, splicing, DNA replication, and DNA repair (Wagner and Carpenter, 2012). So far, a specific role for WHSC1 in the immune defects associated with WHS has not been proven, and, in general, the functions of the members of the NSD family in normal hematopoiesis have not been investigated, even though they are recurrently involved in hematopoietic malignancies (Hu and Shilatifard, 2016). Here, we present in vivo genetic evidence showing that *Whsc1* deficiency impairs normal hematopoietic development at several stages and lineages and particularly affects B cell differentiation and mature B cell function. These findings reveal the role of Whsc1 as a player in hematopoietic development and also indicate that many of the immune defects associated with WHS can be directly attributed to reduced levels of *Whsc1*.

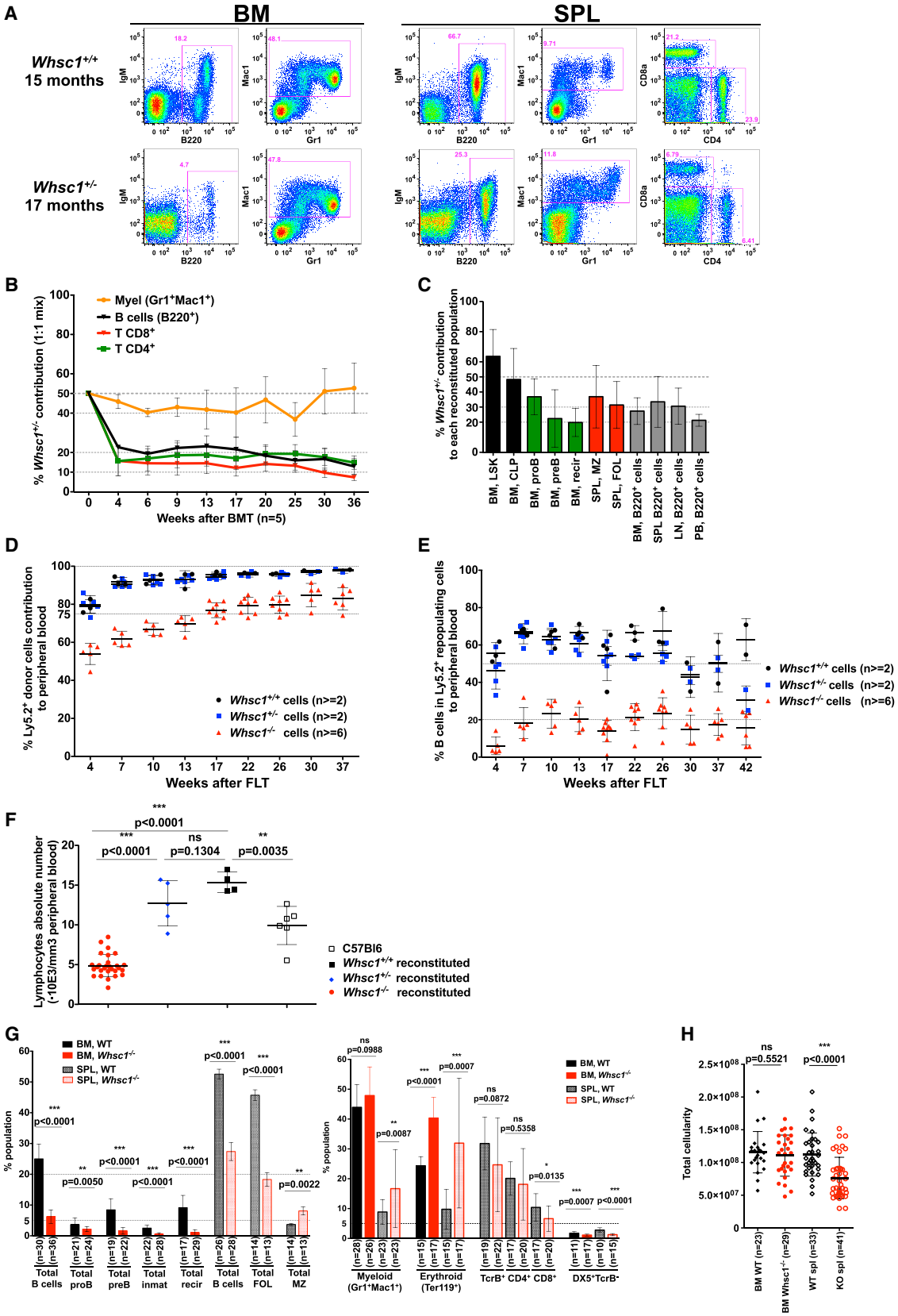

(legend on next page)

RESULTS

Lymphoid Differentiation Is Impaired in *Whsc1* Heterozygous Mice

Since WHS patients lack only one copy of the *WHSC1* gene, we first studied hematopoietic development in heterozygous mice (Nimura et al., 2009). We could not identify any major hematopoietic changes in *Whsc1*$^{+/-}$ mice at 6 months of age (Figure S1A). However, in *Whsc1*$^{+/-}$ mice older than 15 months, a significant decrease in the percentages of B and T lymphocytes (Figure 1A) suggested a progressive defect in the long-term maintenance of the lymphoid compartment.

Competitive bone marrow transplantation (BMT) experiments were performed injecting wild-type (WT) (Ly5.1^{+}) and *Whsc1*$^{+/-}$ (Ly5.2^{+}) cells in a 1:1 ratio into lethally irradiated *Rag1*$^{-/-}$ mice (Figure 1B). In this competitive setting, the developmental defect of *Whsc1*$^{+/-}$ B and T lymphocytes could be appreciated at an early stage (Figure 1B), since they can only contribute to ~20% of the total lymphocytes in peripheral blood (PB). By contrast, the myeloid compartment is maintained at the initial 50:50 ratio, suggesting that its development is not, or only slightly, affected. In order to determine if the *Whsc1*$^{+/-}$ lymphocyte defects could be counterbalanced by increasing their proportion in the mix, injections were performed at a 1:4 WT:*Whsc1*$^{+/-}$ cell ratio (Figure S1B). This resulted in a compensating recovery of the lymphocyte chimerism to a 50:50 ratio. Once more, the myeloid ratios recapitulated those of the original injection ratio.

Full necropsy of 1:1-ratio-injected animals (Figures 1C and S1C) showed that *Whsc1*$^{+/-}$ LSK (lineage-negative, Sca1-positive, cKit-positive) hematopoietic stem/progenitor cells (HSPCs) and common lymphoid progenitors (CLPs) and common myeloid progenitors (CMPs) in the bone marrow (BM) were present at the original 50:50 ratio of injection, like myeloid cells (Figure S1C). However, the *Whsc1*$^{+/-}$ B cell compartments beyond pro-B cells showed a gradual decrease, with the latest stages of B cell development being present only at a 20% ratio, like in the PB (Figure 1C). Therefore, the loss of one copy of *Whsc1* leads to an impairment in lymphoid development that, under normal conditions, only manifests as the mice get older.

Whsc1 Is Required for Normal Hematopoietic Development

Given that *Whsc1*$^{-/-}$ mice die at late gestational stages or in perinatal day 0 (Nimura et al., 2009), in order to study the development of a full *Whsc1*$^{-/-}$ hematopoietic system, we performed embryo fetal liver (FL) transplants. *Whsc1*$^{-/-}$ cells could give rise to all the main types of hematopoietic cells (Figure S2). Therefore, *Whsc1* is not strictly essential for the development of any of the hematopoietic lineages. However, there were differences in the reconstitutive capacity of *Whsc1*$^{-/-}$ cells. First, a kinetic delay could be seen in the repopulation of PB (Figure 1D), mainly due to the 3-fold reduction in the percentages of B220^{+} cells (Figure 1E). Automatic hematic analysis (Figures 1F and S2) confirmed that this 3-fold reduction was also occurring in the absolute numbers of lymphocytes. Fluorescence-activated cell sorting (FACS) analysis showed consistent alterations in different hematopoietic compartments (Figures S3A and 1G); indeed, although total BM cellularity was not affected (Figure 1H), total B cell numbers were 5-fold reduced in the BM of *Whsc1*$^{-/-}$-reconstituted animals. The myeloid compartment was again much less affected, and there was also a significant increase in BM *CD71*$^{+}$*Ter119*$^{+}$ erythroid progenitors (erythroblasts) (Figures S3A and 1G). Within *Whsc1*$^{-/-}$ B cells, the largest decrease took place from pro-B cells onward, suggesting the existence of a non-stringent, leaky, developmental block at the pro-B to pre-B cell transition, allowing the differentiation to later developmental B cell types, albeit in much reduced numbers (Figures S3A and 1G). This was confirmed by the more than 2-fold reduction in the percentages and absolute numbers of B cells in the spleen (Figures 1G and 1H). T cell numbers were also decreased in the absence of *Whsc1* (Figure 1G). In the spleen, there was a strong increase in the percentages of erythroblasts (Figures S3A and 1G), suggesting the presence of extramedullary erythropoiesis. Finally, these alterations also led to a reduction of total cellularity in the spleen of *Whsc1*$^{-/-}$-reconstituted animals (Figure 1H).

Whsc1$^{-/-}$ Hematopoietic Cells Are Totally Outcompeted in the Presence of WT Cells

We performed competitive fetal liver transplant (FLT) experiments in a 1:1 ratio of *Whsc1*$^{-/-}$ (Ly5.2^{+}) cells against WT

Figure 1. Lymphoid and Hematopoietic Differentiation Is Impaired in *Whsc1*$^{+/-}$ and *Whsc1*$^{-/-}$ Cells

(A) Representative FACS plots (out of a total of ten experiments) of aged WT and *Whsc1*$^{+/-}$ mice showing the reduction in the percentages of *Whsc1*$^{+/-}$ B and T cells.

(B) Disadvantage of *Whsc1*$^{+/-}$ hematopoietic cells in a competitive BM reconstitution assay. The vertical axis shows the percentage of contribution of the indicated *Whsc1*$^{+/-}$ cell types to the PB of recipient mice injected with a 1:1 mix of WT:*Whsc1*$^{+/-}$ cells, as determined by flow cytometry of PB samples at the times indicated on the x axis. Mean ± SEM values are shown.

(C) Percentage of contribution of the indicated *Whsc1*$^{+/-}$ cell types in recipient mice injected with a 1:1 mix of WT:*Whsc1*$^{+/-}$ cells, 3–6 months after injection. n = 5 mice for each time point. Mean ± SD values are shown.

(D) Kinetic delay in the reconstitution of the PB cellularity by *Whsc1*$^{-/-}$ cells (red) in comparison with *Whsc1*$^{+/-}$ (blue) or WT (black) cells, monitored by flow cytometry over 30 weeks after FL transplantation. The vertical axis represents the percentage of donor cells in the PB of recipient mice at the indicated time points. n = number of mice analyzed. Mean ± SD values are shown.

(E) Reduced percentage of B cells of *Whsc1*$^{-/-}$ donor origin in PB, with time, as indicated in previous panel. Mean ± SD values are shown.

(F) Reduced absolute numbers of total blood lymphocytes in mice reconstituted with *Whsc1*$^{-/-}$ donor cells, as measured by automatic hematic biometry. Samples are from mice reconstituted with *Whsc1*$^{-/-}$ (red dots), *Whsc1*$^{+/-}$ (blue diamonds), or WT (black filled squares) cells, 2 months after FLT, or from non-reconstituted, normal age-matched C57BL/6 control animals (black hollow squares). Mean ± SD values are shown.

(G) Percentages of the different developmental stages of hematopoietic cells in the BM and spleen from mice reconstituted with either WT or *Whsc1*$^{-/-}$ cells 3–6 months after transplant showing B cell developmental stages (left graph) and other hematopoietic cell types (right graph). Mean ± SD are shown.

(H) Total cellularity of BM and spleen of reconstituted mice. n = number of mice analyzed. Mean ± SEM values are shown.

See also Figures S1–S3.

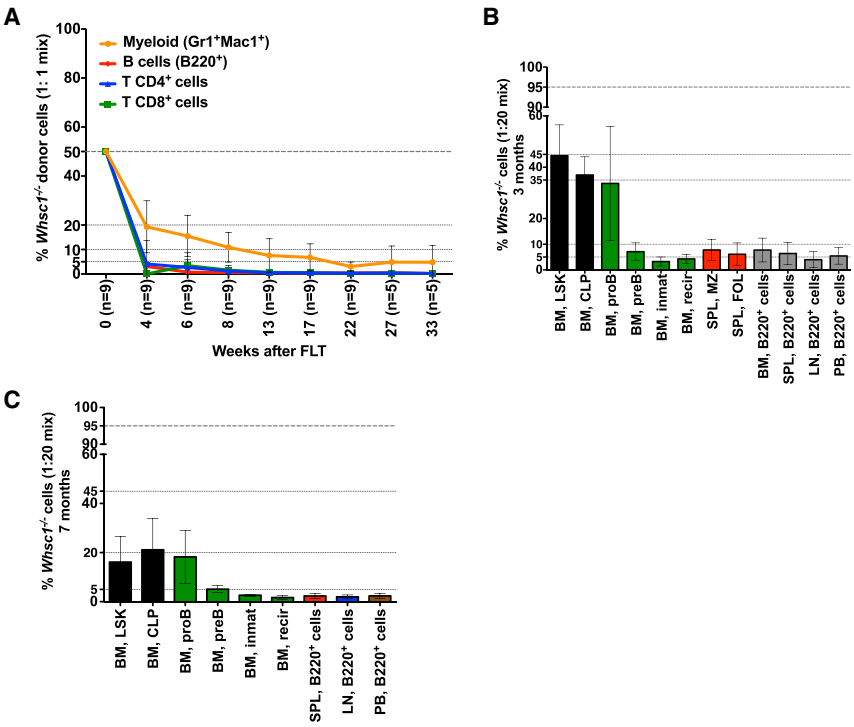

Figure 2. *Whsc1*$^{-/-}$ Cells Are Outcompeted in Competitive Transplantation

(A) Vertical axis shows the drastically reduced percentage of contribution of the indicated *Whsc1*$^{-/-}$ cell types to the PB of recipient mice injected with a 1:1 mix of WT:*Whsc1*$^{-/-}$ cells, as determined by flow cytometry of PB samples at the weeks indicated on the x axis.

(B and C) Percentage of contribution of the indicated *Whsc1*$^{-/-}$ cell types in recipient mice injected with a 1:20 mix of WT:*Whsc1*$^{-/-}$ cells, 3 months (B) or 7 months (C) after injection. The panels show the drastic reduction of B cell developmental stages beyond pro-B cells, and the decrease in LSK cells with time. n = 2 or 5 mice (3 and 7 months, respectively). Mean ± SD values are shown.

See also Figure S2.

(Ly5.1^{+}) cells. All types of *Whsc1*$^{-/-}$ blood cells were totally outcompeted, proving the existence of a developmental disadvantage in all the lineages (Figure 2A). New competitive FLTs were performed in ratios 1:2 or 1:5 (data not shown) and 1:20 (Figure S1D). At this last ratio, *Whsc1*$^{-/-}$ myeloid cells could be found in the blood at an average ratio of 40% and B cells at ~5%. 3 months after the 1:20 transplant, 45% of the LSK population in the BM (Figure 2B) was *Whsc1*$^{-/-}$. The myeloid compartment was present in the same LSK range (Figure S1E). However, B cells beyond the pro-B stage were present at only 5%, as in the blood. 7 months after transplant, *Whsc1*$^{-/-}$ cells comprised only 18% of the LSK population in the BM (Figures 2C and S1F), and so did myeloid cells, while B cells were strongly decreased beyond pro-B cells. These results supported the previously detected developmental impairment at the pro-B to pre-B cell transition and also revealed problems in the maintenance of the *Whsc1*$^{-/-}$ LSK compartment.

Repopulation Capacity Is Impaired in *Whsc1*$^{-/-}$ Hematopoietic Stem Cells

In order to test if there was an impairment in the long-term maintenance of *Whsc1*$^{-/-}$ stem cell function, we performed serial transplantations of WT, *Whsc1*$^{+/-}$, or *Whsc1*$^{-/-}$ BM cells into secondary and tertiary recipients. The Kaplan-Meier survival plot for the tertiary transplant (Figure 3A) shows that *Whsc1*$^{-/-}$ cells have exhausted their repopulation potential, and the majority of the tertiary recipients die quickly due to BM failure (see below). *Whsc1*$^{-/-}$ secondary recipients have no B cells and very few T cells (Figure 3B), confirming that lymphocytes, and especially B cells, are the most severely affected lineage, a fact also supported by the clear reduction in B cell numbers seen in secondary recipients of *Whsc1*$^{+/-}$ cells (Figure 3B) (recapitulating the age-related loss of lymphocytes in *Whsc1*$^{+/-}$ mice; Figure 1A) and by the clear impairment in B cell development beyond pro-B cells in secondary *Whsc1*$^{-/-}$ recipients (Figure S3C). This reduction in B cell numbers was more dramatic in tertiary recipients (Figure 3C). Additionally, the effects of the lack of *Whsc1* in erythropoiesis in the long-term can already be seen in secondary recipients by hematic counting, which shows reductions in hemoglobin, hematocrit, and platelets (Figure S3B). All of these effects indicate an impairment in the repopulation capacity of *Whsc1*$^{-/-}$ hematopoietic stem cells (HSCs). Indeed, when mice with a 1:1 *Whsc1*$^{-/-}$:WT mixture were examined a very short time after reconstitution (2, 4, 7, 15, and 30 days; Figure 3E), *Whsc1*$^{-/-}$ LSK cells and their descendants were quickly outcompeted. Furthermore, FACS analysis of primary recipients (Figure 3D) showed a significant, *Whsc1* dose-dependent reduction in the percentages of LSK cells in the BM.

To discard the idea that the developmental defects we found might be due to transplantation-induced hematopoietic stress, FL, fetal spleen, and fetal thymi of *Whsc1*$^{-/-}$ E18–E21 embryos were analyzed (Figure S3D). In the fetal spleen, the percentage of CD19^{+} cells was reduced by half in *Whsc1*$^{-/-}$ embryos and, in the fetal thymus, a severe reduction in the percentage of CD4-SP cells was evident in heterozygous embryos and dramatic in *Whsc1*$^{-/-}$ embryos. Similar results were found in FL (data not shown), supporting the true nature of the developmental defects identified in our transplantation studies.

Class Switch Recombination Efficiency Is Reduced in *Whsc1*$^{-/-}$ B Cells Due to a Proliferative Defect and Increased Apoptosis

Because WHS patients tend to present with decreased levels of switched immunoglobulins (Hanley-Lopez et al., 1998), and because it was previously shown that WHSC1 facilitates class switching to immunoglobulin A (IgA) in CH12F3 cells in vitro (Pei et al., 2013), we evaluated whether later stages of

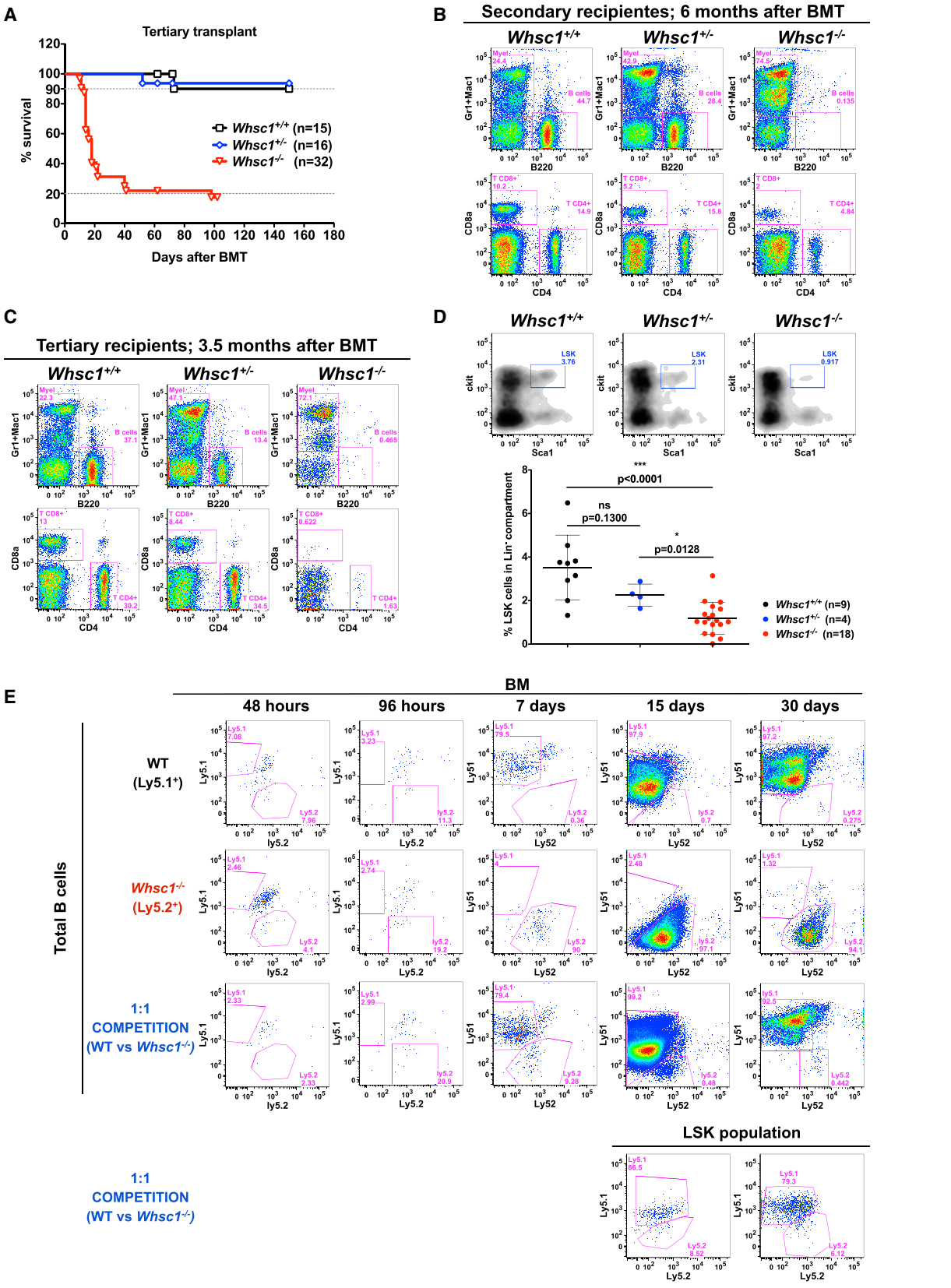

(legend on next page)

lymphocyte development are functionally affected. We performed ex vivo class switch recombination (CSR) experiments in competitive conditions so that equal numbers of splenic B cells of either *Whsc1*$^{+/-}$ or *Whsc1*$^{-/-}$ genotype were plated 1:1 with WT cells (Figure 4) and stimulated with different CSR-inducing stimuli. Both *Whsc1*$^{+/-}$ and *Whsc1*$^{-/-}$ B cells were impaired in their switching to all isotypes in all conditions tested (Figure 4A). This was confirmed by in vivo sheep red blood cell (SRBC) immunization of reconstituted mice (Figures 4B and 4C), showing that the percentage of switched cells at 13 days was greatly reduced in both *Whsc1*$^{+/-}$ and *Whsc1*$^{-/-}$ cells. ELISA assays showed a reduction in the serum levels of switched IgG1 in *Whsc1*$^{-/-}$-reconstituted, SRBC-injected mice (data not shown), although both *Whsc1*$^{+/-}$ and *Whsc1*$^{-/-}$ cells could give rise to splenic plasma cells (Figure 4D). All of these results show that in vivo, in lymphocytes in a genetic model, *Whsc1* is required for an efficient CSR to most of the isotypes, providing a model that really recapitulates one of the most serious complications faced by WHS patients.

Since CSR is linked to cellular proliferation, ex vivo competitive assays were carried out after labeling the cells with CellTrace in order to follow the different cycles of division. The contribution of *Whsc1*$^{-/-}$ cells was strongly reduced in all generations, and at the end, it accounted for a very reduced percentage (Figures 4E, 4F, and S4), and absolute number (Figure 4G) of cells, supporting the existence of a proliferative impairment in *Whsc1*$^{-/-}$ cells. FACS analysis also showed (Figure 4H) increased levels of apoptosis in stimulated *Whsc1*$^{-/-}$ B cells.

Cell-Cycle Alterations in *Whsc1*$^{-/-}$ B Cells and HSPCs

We performed cell-cycle analysis in the presence of bromodeoxyuridine (BrdU) during the CSR reaction. After 72 hr under stimulation, in all the different cell generations, there was a 3-fold increase in the number of cells in the S phase of the cell cycle in *Whsc1*$^{-/-}$ B cells (Figures 5A and S5A). To investigate whether this alteration was also present in vivo at the other developmental points where we had found that the absence of *Whsc1* led to important malfunctions, we performed in vivo BrdU labeling. The results showed that in the BM, both B cells at all of the different developmental stages (Figures 5B and 5F) and LSK cells (Figure 5C) showed an increased number of BrdU^{+} S phase cells, while *Whsc1*$^{-/-}$ myeloid cells did not present any alteration (Figure 5B).

It has been reported that changes in the pattern of methylation at H3K36 can affect DNA repair (Wagner and Carpenter, 2012), and WHSC1 has been associated with DNA damage repair (Evans et al., 2016; Hajdu et al., 2011; Shah et al., 2016). We studied the levels of γH2AX, a well-known indicator of the existence of broken DNA ends. In the context of the CSR reaction (Figures 5D, S5B, and S5C), we could see progressively increased levels of γH2AX during the successive generations in *Whsc1*$^{-/-}$ cells, and this correlates with the accumulation of cells in S phase. Furthermore, also in vivo, a slight elevation in γH2AX levels can be appreciated in *Whsc1*$^{-/-}$ total B cells in the BM, especially when compared with *Whsc1*$^{-/-}$ myeloid cells that, once more, seem to be unaffected (Figure 5E). Also, a similar increase in γH2AX levels could be detected in BM *Whsc1*$^{-/-}$ LSK cells (Figure 5E). These same results could be found in a totally different cell type, *Whsc1*$^{-/-}$ mouse embryo fibroblasts (MEFs), which also presented a very compromised proliferative capacity (Figure 5G) and severe impairment in the downregulation of γH2AX levels after DNA damage (gamma irradiation instead of CSR, in this case) (Figure 5H).

Whsc1$^{-/-}$ GC B Cells Present Severe Alterations in Many Basic Cellular Processes

We next studied the variations in the transcriptome in proliferative *Whsc1*$^{-/-}$ GC (germinal center) cells versus WT cells. We used RNA sequencing (RNA-seq) to compare *Whsc1*$^{-/-}$ and WT ex vivo lipopolysaccharide (LPS)-stimulated splenic B cells (Figures 6A and S6; Tables S1, S2, and S3). The results demonstrate the existence of severe defects at many key levels of cellular biology. First, a basic differential gene expression analysis showed that there are several developmental genes deregulated in the absence of Whsc1, like the genes of the *Hoxa* cluster (Figure S6A; Tables S1 and S2). These developmental genes, although of great importance to the morphogenetic pathways affected in WHS patients, do not explain the B cell phenotypes that we have described. However, using pathway analysis, we observed that many key processes, such as the cell cycle, splicing, ribosome synthesis, DNA replication, or DNA repair, are very significantly altered in proliferating *Whsc1*$^{-/-}$ B cells (Figure 6A; Table S3). Functional analysis using gene set enrichment analysis (GSEA) (Figures 6B and S6B) confirmed these findings. Indeed, although B cell-specific pathways are also affected (Figures 6B and S6B, "BCR signaling"), and this could

Figure 3. Impaired Functionality of *Whsc1*$^{-/-}$ HSCs

(A) Kaplan-Meier survival plot of recipients of a 3^{ary} serial BMT of cells of the indicated genotypes showing the exhausted reconstitutive capacity of *Whsc1*$^{-/-}$ cells. n = number of transplanted animals.

(B) PB from mice reconstituted with a secondary serial transplant of WT, *Whsc1*$^{+/-}$, or *Whsc1*$^{-/-}$ cells 6 months after transplant. Data shown are representative FACS plots out of at least 14 *Whsc1*$^{+/-}$ and 31 *Whsc1*$^{-/-}$-reconstituted mice, independently analyzed, from three different donors.

(C) PB from mice reconstituted with a tertiary serial transplant of WT, *Whsc1*$^{+/-}$, or *Whsc1*$^{-/-}$ cells 3.5 months after transplant. Data shown are representative FACS plots out of at least 8 *Whsc1*$^{+/-}$ and 17 *Whsc1*$^{-/-}$-reconstituted mice, independently analyzed, from three different donors.

(D) Percentages of LSK cells in the BM of recipients of cells of the indicated genotypes 6–8 weeks after transplantation with FL cells from littermate embryos of the indicated genotypes. FACS plots are representative of the data summarized in the graph below (mean ± SD).

(E) Short-term engraftment of *Whsc1*$^{-/-}$ cells into irradiated Ly5.1/Ly5.2 heterozygous recipients. First two rows show the kinetics of short-term B cell reconstitution in the BM of mice injected with either WT or *Whsc1*$^{-/-}$ cells. FACS plots are gated in total B220^{+} cells. Third row shows competitive kinetics of short-term B cell reconstitution in the BM of mice injected with a 1:1 mix of WT:*Whsc1*$^{-/-}$ cells. FACS plots are gated in total B220^{+} cells. The bottom row shows kinetics of short-term reconstitution, at 15 and 30 days, of LSK cells in the BM of mice injected with a 1:1 mix of WT:*Whsc1*$^{-/-}$ cells. The whole experiment was repeated twice with similar results.

See also Figure S3.

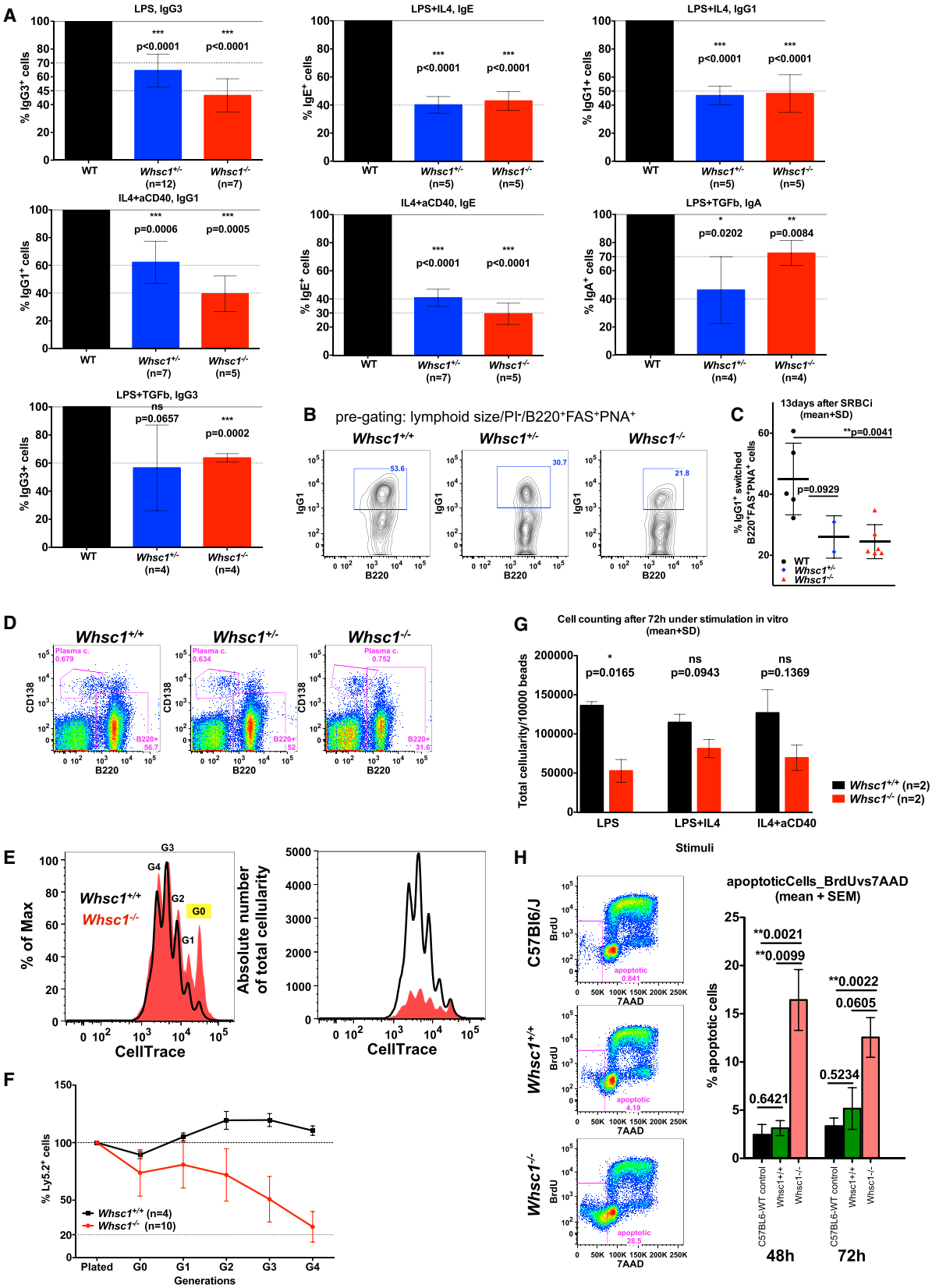

(legend on next page)

explain some aspects of the developmental B cell impairment, the downregulation of ribosomal proteins, the upregulation of the components of the spliceosome or of cell cycle genes (Figures 6A and 6B) are directly related to all the cellular phenotypes described. In concordance with the accumulation of γH2AX, a very strong deregulation of the genes involved in DNA repair could be seen (Figures 6B and S6B). Among them, there was an upregulation of the Fanconi anemia pathway, which is involved in the repair of DNA damage associated with DNA replication (Kais et al., 2016). In fact, one of the most significantly altered pathways was the one regulating DNA replication (Figures 6B and S6B), therefore pointing toward this process as a potential trigger of the abnormal proliferative behavior of *Whsc1*$^{-/-}$ cells.

Absence of Whsc1 Leads to Increased DNA Replicative Stress in GC B Cells

In some cell lines, Whsc1 is associated with DNA damage repair (Evans et al., 2016; Hajdu et al., 2011; Shah et al., 2016). Also, cell lines derived from WHS patients present delayed cell-cycle progression and impaired DNA replication (Kerzendorfer et al., 2012), but which gene is responsible for this phenotype among the many genes lost in WHS is not yet clear. It has been shown that correct H3K36me3 patterns are required to prevent replicative stress in cancer cells lines (Kanu et al., 2015), and H3K36 demethylation has been shown to control proliferation, the cell cycle, and hematopoietic development (Andricovich et al., 2016; He et al., 2008). Therefore, as suggested by the RNA-seq results, we decided to test in our in vivo model whether the proliferative impairment could be due to increased levels of DNA replicative stress. We performed DNA fiber analysis (Flach et al., 2014) in *Whsc1*$^{-/-}$ MEFs and stimulated B cells. There was a reduction in both the fork rate and the inter-origin distances in the absence of *Whsc1* (Figure 6C), confirming an impairment in the advancement of the replication fork, coupled with the activation of new dormant origins. We also cultured cells in the presence of increasing concentrations of the DNA replication inhibitor aphidicolin (Figures S5D and S5E). *Whsc1*$^{-/-}$ cells were more affected by aphidicolin than WT cells (Figure S5D), but, more significantly, cell cycle analysis showed that in the presence of aphidicolin, *Whsc1*$^{-/-}$ B cells could not correctly exit S phase (Figure S5E), presenting a prolonged S phase without properly entering G2/M. These results confirm that replication stress is the main molecular mechanism behind proliferative impairment in the absence of *Whsc1*.

Specification and Commitment to the B Cell Lineage Are Strongly Impaired in *Whsc1*$^{-/-}$ B Cell Progenitors

In order to identify whether the impairment in the pro-B to pre-B cell transition was due to the same molecular mechanism, we sorted BM pro-B cells and performed RNA-seq followed by differential gene expression and GSEA. We found that *Whsc1*$^{-/-}$ pro-B cells share some of the defects found in GC B cells but with different severity, and, more significantly, they also present pro-B cell stage-specific transcriptional defects (Tables S4, S5, and S6; Figures 7 and S7). Indeed, *Whsc1*$^{-/-}$ pro-B cells also present significant alterations in DNA repair, DNA replication, and cell cycle gene sets (Figures 7A and S7A) and downregulation of genes involved in nucleosome and chromatin organization (Figures 7A and S7A). Since there was no statistically significant difference in the percentage of cells in S phase between WT and *Whsc1*$^{-/-}$ BM pro-B cells (Figure 5F), these RNA-seq differences most likely reflect intrinsic, cell-specific differences between the two genotypes; there was a significant downregulation of key early B cell developmental genes (Table S5), including *Ikzf3*, *Tcf3*/*E2a*, *Ebf1*, *Pax5*, *Rag1*, *Rag2*, *Il7r*, and *Foxo1*, and this was particularly important in the case of *Ebf1* (16-fold downregulated in *Whsc1*$^{-/-}$ cells) and *Pax5* (9.5-fold downregulated). Since these genes are key regulators of the specification and commitment to the B cell lineage (Cobaleda et al., 2007), we generated specific genes sets with the most relevant of their published targets (Pongubala et al., 2008; Revilla-I-Domingo et al., 2012; Treiber et al., 2010) and evaluated them by GSEA (Figures 7B, 7C, and S7B). The results showed a strong downregulation of a significant majority of the Ebf1- and Pax5-upregulated target genes in *Whsc1*$^{-/-}$ pro-B cells, affecting most of

Figure 4. Impaired CSR in *Whsc1*$^{-/-}$ B Cells

(A) Differences in the percentages of class-switched B cells depending on their genotype, expressed as percentages relative to WT cells (left black bar, 100%). The stimuli used and the switched immunoglobulin subtypes measured are indicated. n = number of independent experiments performed. p values refer to a two-sided Student's t test versus WT. Mean ± SD values are shown.

(B) Reduction of in vivo splenic Ig-switched GC B cells (pre-gated as B220$^+$,PNA$^+$,FAS$^+$) in *Whsc1*$^{+/+}$, *Whsc1*$^{+/-}$, or *Whsc1*$^{-/-}$ recipients. Spleens were analyzed 13 days after immunizing with SRBCs recipient mice reconstituted with cells of the indicated phenotypes. FACS plots are representative of the data summarized in the graph shown in the next panel (mean ± SD).

(C) Graphical representation and statistical analysis of the percentages of in vivo IgG1$^+$ cells for each genotype. Mean ± SD values are shown.

(D) *Whsc1*$^{-/-}$ cells can give rise to plasma cells; representative FACS plots are shown from three independent replicate experiments analyzing the spleen of mice reconstituted with the indicated genotypes.

(E) FACS histogram showing the deconvolution, after 72 hr of stimulation with LPS, of the total cellular population in the different generations of cells using the dilution of the CellTrace dye to separate the cells according to the number of times they have divided. The y axis scale is expressed as percentage related to the maximum in the left histogram and as absolute numbers of cells in the right histogram. G0–G4 indicates generations of cells.

(F) Evolution of the percentage of either WT or *Whsc1*$^{-/-}$ ex vivo LPS-stimulated Ly5.2$^+$ B cells, in competition against WT Ly5.1$^+$ B cells, along the different generations and relative to the initial percentage when plated. Mean ± SD values are shown.

(G) Reduced absolute numbers of *Whsc1*$^{-/-}$ cells obtained 72 hr after stimulation of splenic B cells in absence of competition, in the presence of a defined number of microbeads.

(H) Percentages of apoptotic B cells after 48 hr or 72 hr in culture under LPS-stimulation. Left: gating strategy and representative plots of cells after 48 hr in culture. C57Bl6 refers to cells from WT non-reconstituted animals (n = 7), while the other two lanes show plots of mice reconstituted with either WT (n = 3) or *Whsc1*$^{-/-}$ (n = 9) cells. Right: bar graph plot summarizing the data.

See also Figure S4.

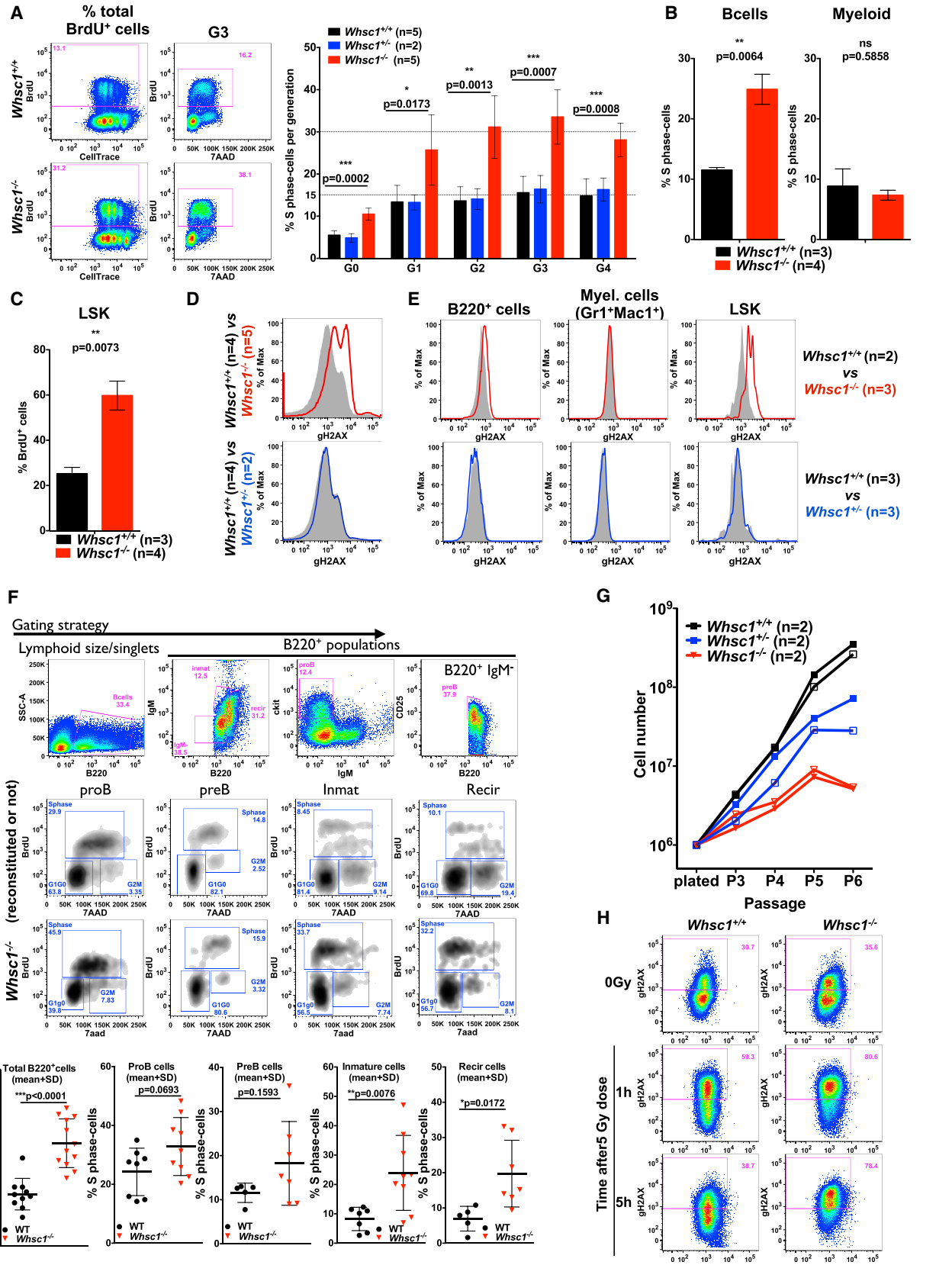

(legend on next page)

the biological processes necessary for the specification and commitment of progenitors to the B cell lineage (Cobaleda et al., 2007). These data therefore correlate with the developmental block at this early phase of B cell differentiation and show that Whsc1 participates in different mechanisms that control differentiation and function at several stages of B cell life.

DISCUSSION

An increased susceptibility to infections is one of the main pathological characteristics affecting WHS patients, and the molecular basis for this immunodeficiency is so far unknown. Here, we present in vivo genetic evidence of the involvement of the *Whsc1* gene in hematopoietic development and in B cell differentiation and function at several stages of differentiation. Importantly, we show the existence of an impairment in the development of *Whsc1*$^{+/-}$ lymphocytes that manifests subtly, but progressively, with age. This finding could have serious implications for the long-term prognosis of immunodeficiency in WHS patients (hemizygous for *WHSC1*), because it implies that their immune response at late stages of life might be seriously impaired.

The total loss of *Whsc1* affects the development and function of different blood cell types, especially HSPCs and B cells at several developmental stages. There is a strong block at the pro-B to pre-B cell transition. Blocked *Whsc1*$^{-/-}$ pro-B cells have severely reduced levels of the key B cell transcription factors *Ebf1* and *Pax5*. This correlates with global downregulation of Ebf1 and Pax5 positively regulated target genes necessary for controlling essential molecular aspects of early B cell development: immunoglobulin genes (Figures 7B, 7C, S7B, and S7C); receptors, signal transducers, and kinases (e.g., *Blnk*, *Bcar3*, and *Cd19*); or transcription factors and nuclear proteins (e.g., *Bach2*, *E2f2*, *Rb1*, and *Lef1*). The combined decreased expression of early B cell transcriptional regulators has been previously shown to interfere with normal development of the B cell lineage (Ungerbäck et al., 2015). We tried to rescue this pro-B to pre-B cell block by breeding *Whsc1*$^{-/-}$ mice with animals carrying a rearranged $V_HD_HJ_H$ gene (B1-8) inserted in the JH locus (B1-8i) (Sonoda et al., 1997). However, this, by itself, was not enough to overcome the block (Figure 7D), confirming its dependence on many deficient signaling molecules and B cell-specific factors beyond immunoglobulin rearrangements. In summary, *Whsc1*$^{-/-}$ cells can generate CLPs, pro-B cells, and later B cell stages too, but they do not do this efficiently; in the absence of competition, impairment exists, but it is leaky and allows for the generation of mature B cells, although with a much reduced efficiency. Therefore, B cell specification and commitment can take place in the absence of Whsc1, but these processes are seriously compromised and become insufficient when challenged in any way.

Regarding later stages of B cell development, we could also show that there is an impairment in the CSR reaction that is dose dependent in relation to the absence of the *Whsc1* alleles. This is related to an aberrant proliferation of *Whsc1*-deficient cells, which showed a 3-fold increase in the percentage of cells in S phase, coupled with an accumulation of DNA damage. *Whsc1*-deficient cells have large deregulations of gene sets involved in key biological processes, among them the genes involved in DNA repair and DNA replication. They also show a significantly decreased fork rate counteracted by local increases in origin density, suggesting that a higher frequency of stalled forks induces compensatory activation of dormant origins and triggers a DNA damage response (Maya-Mendoza et al., 2009). The fact that the Fanconi anemia (FA) pathway (responsible for repairing DNA as a response of replication stress; Kais et al., 2016) is significantly altered further supports this idea. This replicative stress leads to the accumulation of DNA damage, as indicated by increased γH2AX levels; however, this does not result in increased numbers of chromosomal aberrations as measured by DNA FISH on the immunoglobulin locus (C.C. and J.A.K., unpublished data). There is also an accumulation of

Figure 5. Cell-Cycle Alterations and DNA Damage Accumulation in *Whsc1*$^{-/-}$ Cells

(A) FACS analysis of cell cycle in ex vivo LPS-stimulated, BrdU-labeled B cells. 72 hr after stimulation, cell culture medium was supplemented with BrdU and cells were harvested 1 hr later. Leftmost panels show the total incorporation of BrdU and the dilution of CellTrace. Central panels display the cell cycle profile (BrdU versus 7AAD) for the generation 3 (G3) of cells showing the 3-fold increased percentage of *Whsc1*$^{-/-}$ cells in S phase. Bar graph shows the percentage of cells in S phase for each generation for the three indicated genotypes. Bars represent mean ± SD; n = number of independent experiments.

(B) 3-fold increased percentage of *Whsc1*$^{-/-}$ total B cells in the S phase in vivo in the BM, and absence of changes in myeloid cells. Mice were intraperitoneally injected with BrdU and sacrificed after 2 hr. Bar graphs represent the mean ± SD.

(C) Increased BrdU incorporation in vivo by BM *Whsc1*$^{-/-}$ LSK cells. Bar graphs represent the mean ± SD.

(D) Histograms showing the increased levels of γH2AX accumulation in ex vivo LPS-stimulated *Whsc1*$^{-/-}$ B cells in comparison with either WT or *Whsc1*$^{+/-}$ B cells, as determined by flow cytometry.

(E) Increased levels of γH2AX in vivo in total BM *Whsc1*$^{-/-}$ B cells and LSK cells in comparison with WT counterparts. *Whsc1*$^{-/-}$ myeloid cells do not present abnormal γH2AX levels, and neither do *Whsc1*$^{+/-}$ BM cells. Representative plots are shown.

(F) Cell-cycle analysis through the different stages of B cell development in the BM. Top row: gating strategy for BM B cell compartments (cells were fixed for cell cycle studies). Middle rows: representative FACS plots for WT and *Whsc1*$^{-/-}$ cells. Bottom graphs: percentages of cells in S phase for the indicated BM B cell compartments, as determined by in vivo incorporation of BrdU.

(G) Impaired proliferation of *Whsc1*$^{+/-}$ and *Whsc1*$^{-/-}$ MEFs. Growth curves of freshly prepared MEFs of the indicated genotypes showing the reduced proliferative capacity of *Whsc1*$^{-/-}$ cells. Representative analyses are shown out of three independent experiments with a total of 17 MEF preparations (4 *Whsc1*$^{+/+}$, 5 *Whsc1*$^{+/-}$, and 8 *Whsc1*$^{-/-}$ embryos).

(H) Impaired DNA damage repair in *Whsc1*$^{-/-}$ MEFs. WT and *Whsc1*$^{-/-}$ MEFs were irradiated with 5 Gy and γH2AX levels were measured after 1 and 5 hr. *Whsc1*$^{-/-}$ MEFs cannot efficiently remove gamma-irradiation-induced γH2AX accumulation, while levels of γH2AX have reverted to normal in WT MEFs within 5 hr after exposure. One representative analysis is shown out of three independent experiments with a total of 12 MEF preparations (6 *Whsc1*$^{+/+}$ and 6 *Whsc1*$^{-/-}$ embryos).

See also Figure S5.

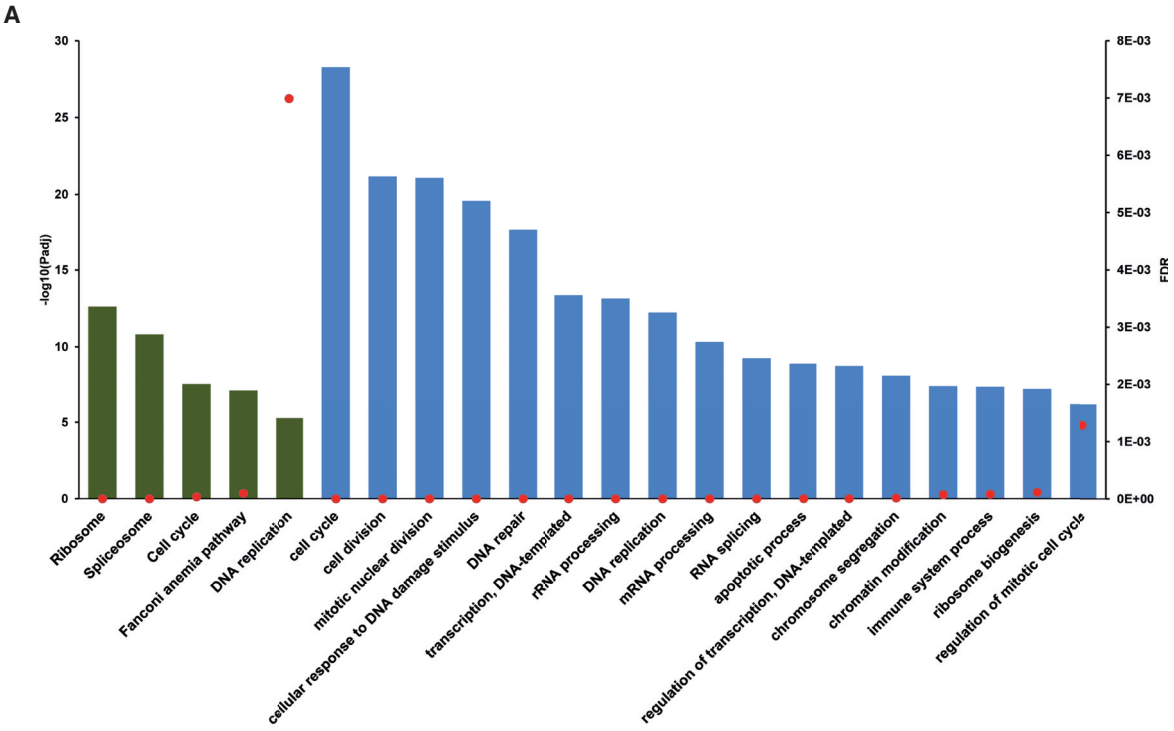

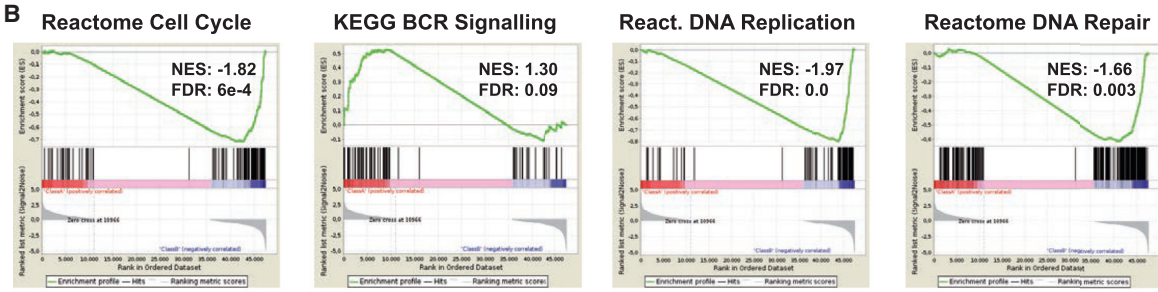

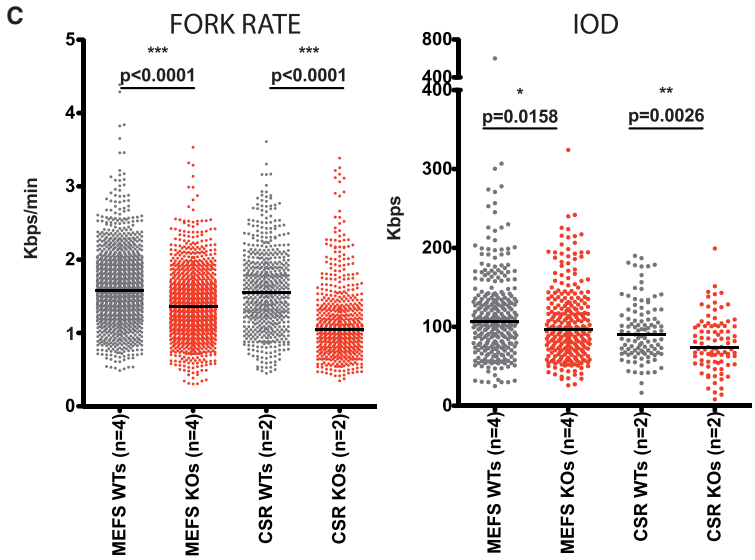

(legend on next page)

Whsc1-deficient apoptotic cells (Figure 4H), suggesting that those cells that cannot cope with the replication stress die and, in the surviving cells, the increased DNA repair mechanisms, together with the increased numbers of replication origins and an elongated S phase, allow them to correctly finish the cell cycle, although the global fitness of the population is severely affected, as shown by all the different competition experiments. Additionally, one of the cellular components most affected by replicative stress is the ribosome, both at the rRNA and protein levels (Golomb et al., 2014), and stimulated *Whsc1*-deficient cells show a massive downregulation of the expression of integral ribosomal proteins, most likely as a reflection of this fact.

According to the methyltransferase activity of Whsc1, it has been demonstrated in different tumor-related experimental settings that alteration of WHSC1 activity levels leads to parallel global changes in the patterns of H3K36 methylation (García-Carpizo et al., 2016; Kuo et al., 2011; Oyer et al., 2014; Popovic et al., 2014). In our *Whsc1*$^{-/-}$ mouse model, it has already been shown by western blot and immunohistochemistry that the levels of H3K36 methylation are reduced in *Whsc1* knockout (KO) cells (Nimura et al., 2009; Sarai et al., 2013). Therefore, the changes in gene expression revealed by RNA-seq experiments are most likely downstream of changes in H3K36 methylation patterns and include indirect effects of an altered epigenetic landscape. In the context of B cell differentiation, the pro-B to pre-B transition and the germinal center reaction are the two stages corresponding to the maximum peaks of expression of *Whsc1* in hematopoiesis (http://www.immgen.org; Heng and Painter, 2008), suggesting that the high levels of *Whsc1* expression makes these cells particularly vulnerable to the loss of this gene. Conversely, comparative RNA-seq analysis of gene expression in non-proliferative, ex-vivo-sorted, resting lymph node B cells (data not shown; two WT versus four KO samples) did not show any significant changes in the pathways that were greatly altered in proliferative CSR B cells or pro-B cells, only in some of the morphogenetic developmental genes.

We also found the existence of a stem cell functional defect in the absence of Whsc1. First, there was a dose-dependent decrease in the percentage of LSK cells in the absence of Whsc1 (Figure 3D). Since the total BM cellularity was relatively constant between WT and *Whsc1*$^{-/-}$ animals (Figure 1H), it can therefore be concluded that the absolute number of LSK cells is significantly decreased in *Whsc1*$^{-/-}$ mice. Second, in competitive FL transplantations mixing WT and *Whsc1*$^{-/-}$ cells at a 1:20 ratio (Figures 2 and S1), the percentage of *Whsc1*$^{-/-}$ LSK cells steadily decreased over time (45% at 3 months and 18% at 7 months). Third, the serial transplantation experiments led to BM failure and death in tertiary recipients (Figure 3A), a paradigmatic demonstration of stem cell failure. Fourth, the presence of a 3-fold increased percentage of BrdU^{+} (S phase) cells in *Whsc1*$^{-/-}$ BM LSKs (Figure 5C) is indicative of a cell-cycle problem similar to the one observed in stimulated (CSR) B cells or BM B cells. Fifth, the unresolved accumulation of γH2AX in *Whsc1*$^{-/-}$ BM LSKs was similar to that observed in stimulated (CSR) B cells, BM B cells (Figure 5E), and irradiated *Whsc1*$^{-/-}$ MEFs (Figure 5H). The data from CSR B cells show that this increased γH2AX correlates with increased replicative stress and an increased percentage of cells in S phase. Correspondingly, the data from MEFs show that *Whsc1*$^{-/-}$ MEFs are almost non-proliferative in culture (Figure 5G) and have increased DNA replicative stress (Figure 6C) and impaired DNA repair (Figure 5H). Finally, the results from short-term analysis of mice transplanted in a 1:1 WT:*Whsc1*$^{-/-}$ competition (Figure 3E) show that *Whsc1*$^{-/-}$ LSK cells are quickly outcompeted after transplant. All of this functional and cellular evidence strongly suggests that *Whsc1*$^{-/-}$ HSPCs have a cell-cycle disadvantage that leads to a progressive reduction in their numbers with time. This reduced fitness becomes quickly evident when *Whsc1*$^{-/-}$ cells are challenged in a serial transplantation or in a competitive setting. However, any number of events, such as reduced numbers, impaired homing, altered self-renewal potential, or abnormal differentiation, could account for the impaired reconstituting potential of Whsc1-deficient HSPCs, and this should be the focus of future work.

Altogether, our results show that Whsc1 is involved in hematopoietic development at several stages and implicate different cellular lineages. Furthermore, Whsc1 participates in the regulation of different molecular mechanisms throughout these different stages and cell types, from HSC function to B cell lineage specification and commitment, fitness, and cellular proliferation. Our results highlight Whsc1 as a player in the control of hematopoietic and especially B cell development, and they also indicate that the immune defects associated with WHS can be directly attributed to reduced levels of *Whsc1*. These findings provide a framework for the understanding, prognosis, and potential future treatment of immunodeficiency in WHS.

EXPERIMENTAL PROCEDURES

Mice

The following mice were maintained in the C57BL/6 background and, when required, genotyped as described previously: *Whsc1*$^{-/-}$ (Nimura et al.,

Figure 6. Severe Alteration of Biological Processes in *Whsc1*$^{-/-}$ GC B Cells

(A) Threshold-based functional pathway analysis for the differentially expressed genes in GC B cells (*Whsc1*$^{-/-}$ versus WT) with DAVID. Selected KEGG (green) and GO (blue) pathways are represented. Bars represent the antilogarithm of the adjusted p value (left vertical axis). Red dots represent the false discovery rate for the corresponding pathways (right vertical axis).

(B) Gene set enrichment analysis (GSEA) plots for the indicated gene sets (see their corresponding heatmaps in Figure S6B). The GSEA comparison was performed (WT minus *Whsc1*$^{-/-}$), so the genes downregulated in the *Whsc1*$^{-/-}$ cells appear at the left of the scale on each graph, and those upregulated appear at the right side. Therefore, gene sets downregulated in *Whsc1*$^{-/-}$ cells have a positive normalized enrichment score (NES), and gene sets upregulated in *Whsc1*$^{-/-}$ cells have a negative NES.

(C) Impaired DNA replication of *Whsc1*$^{-/-}$ MEFs and CSR B cells, as determined by DNA fiber analysis. FR (left) in kilobase pairs (Kbps)/min, and inter-origin distance (IOD; right) in Kpbs were measured for either MEFs (two leftmost columns in every graph) or CSR-stimulated B cells (two right columns) for WT (gray) or *Whsc1*$^{-/-}$ (red) cells. n = number of different clones (donors). Horizontal bar represents the median for each data column.

See also Figures S5 and S6.

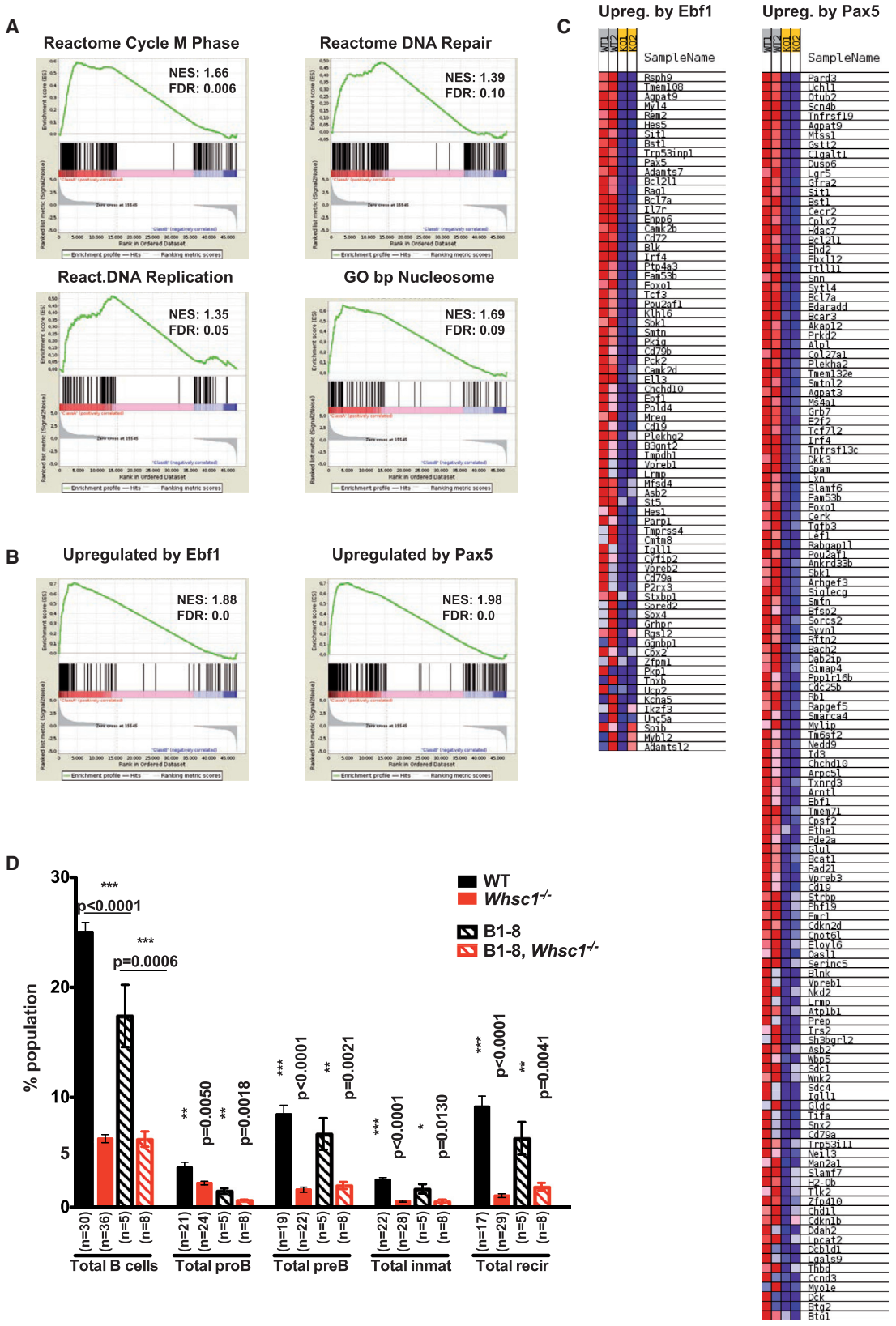

(legend on next page)

2009), *Rag1*$^{-/-}$ (Mombaerts et al., 1992), and *B6.SJL-PtprcaPep3b/BoyJ*. All mice were housed in a specific-pathogen-free (SPF) barrier facility. All experimental procedures conducted on mice were approved by the CBMSO's Institutional and Spanish Regional Committees on Ethics of animal research. Mice with the indicated genotypes were included in the study without any further preselection or formal randomization and with balanced numbers from both genders; we used age-matched mice. Investigators were not blinded to genotype group allocations. All mice were maintained in C57BL/6J background.

FACS Analysis and Sorting Purification

Contaminating red blood cells were lysed using ACK Lysing Buffer. The remaining cells were washed in FACS buffer (1× PBS with 2% heat-inactivated fetal bovine serum [HI-FBS]). After staining, all cells were washed once in FACS buffer and resuspended in the same buffer containing 2 mg/mL propidium iodide (PI) to allow dead cells to be excluded. The samples and the data were acquired in a FACSCantoII Flow Cytometer, sorted in FACSAria Fusion, and analyzed using FlowJo software (Tree Star). Preincubation of cells with CD16/CD32 (2.4G2) Fc-block solution (BD Biosciences) was used to avoid nonspecific antibody binding. BM pro-B cells were purified in a FACSAria Fusion (BSII, Becton Dickinson) as B220^{+} CD19^{+} c-Kit^{+} CD25^{-} PI^{-}. The different antibodies used and the surface markers defining the different populations are indicated in Supplemental Experimental Procedures.

FL or BM Transplantation Experiments

Total BM cells (flushing from the long bones) or FL cells (taken from E21 embryos or P0 newborns) were injected intravenously into lethally irradiated recipients, either *Rag1*$^{-/-}$ (Ly5.2^{+}), or B6.SJL-PtprcaPep3b/BoyJ Ly5.1^{+} or Ly5.1^{+}/Ly5.2^{+} WT, depending on the experiment. For all transplantations, total BM or FL donor cells were counted using a handheld automated cell counter (Scepter, 40 μm tips; EMD Millipore), and the injection ratio was checked by flow cytometry.

Proliferation, Damage, and Cell-Cycle Analysis

The Apoptosis, DNA Damage and Cell proliferation Kit (catalog number 562253, BD Pharmingen) was used to assess the proliferative capacity of the cells, as well as cell-cycle dynamics and DNA damage accumulation. Anti-BrdU-FITC or Anti-BrdU-APC versus 7AAD were used to study the cell cycle, and the CellTrace Violet Cell Proliferation Kit (catalog number C34557, Invitrogen) was used to monitor cell proliferation. CountBright Absolute Counting Beads for flow cytometry (MP 36950, Molecular Probes, Invitrogen) were used to measure absolute cell yield in culture.

CSR Assays

Mouse primary B cells were purified from the spleens of the indicated strains of mice by immunomagnetic depletion with anti-CD43 beads (Miltenyi Biotec) and cultured in 50 μM 2-β-mercaptoethanol (Invitrogen), 10 mM HEPES (Invitrogen), 1 mM glutamine, antibiotics, non-essential amino acids, and 10% HI-FBS RPMI medium supplemented with (1) 25 μg/mL LPS (Sigma-Aldrich), (2) 25 μg/mL LPS and 20 ng/mL interleukin 4 (IL-4) (PeproTech), (3) 25 μg/mL LPS and 2 ng/mL TGF-Beta1 (R&D Systems), or (4) 20 ng/mL IL-4 (PeproTech) and 1 μg/mL anti-CD40 (eBioscience) or non-supplemented (only growth medium). Cells were counted using a handheld automated cell counter (Scepter, 40 μm tips), and the CellTrace Violet Cell Proliferation Kit was used as proliferation tracer.

RNA Extraction

Proliferating B cells were obtained by in vitro LPS stimulation over a 72-hr period as previously described. BM pro-B cells were sorted as previously described. Sorting strategy and purity are shown in Figure S7D. RNA was extracted using a commercial TRIzol reagent (catalog number 15596-026, Life Technologies, Gibco) according to the manufacturer's recommendations. Chemical quality was measured with a Nanodrop 1000 Spectrophotometer (Thermo Scientific), and integrity was confirmed using the Agilent 2100 Bioanalyzer. Libraries for RNA-seq were prepared as indicated in Supplemental Experimental Procedures.

DNA Fiber Spread

Replication track analyses were performed as described previously (Flach et al., 2014), with only minor modifications. MEFs were traced at exponential growth during their third passage, and proliferating B cells were obtained after 48 hr of in vitro culture under LPS stimulation. Both cell types were incubated for 20 min with each thymidine analog (first 5-Chloro-2′-deoxyuridine [CldU] and then 5-Iodo-2′-deoxyuridine [IdU]) and washed three times with warm 1× PBS (37°C). Spreading buffer incubation was for 6 min, primary antibody incubation timing was extended to overnight, and secondary antibody incubation was 2 hr. Tracks were imaged on a fluorescence resonance energy transfer (FRET) Zeiss microscope coupled to a Hamamatsu camera. All pictures were taken at 40× magnification. Fork rate (FR) and inter origin distance (IOD) were calculated based on the length of the IdU tracks measured using ImageJ software and the already published formulas fork rate (kb min^{-1}) = (2.59 (kb μm^{-1}) × length (μm)/ pulse time (min)) and IOD (kb) = length between two contiguous origins (μm). When aphidicolin was used, it was added at 1 μg/mL with the second pulse of thymidine analog (IdU).

Statistical Analysis

Exact sample sizes and statistical tests used for comparisons are indicated in each figure. Kaplan-Meier survival curves were created and analyzed using Prism (GraphPad Software), which used the log-rank test to calculate significance. Samples were allocated to their experimental groups according to their predetermined type (i.e., mouse genotype), and, therefore, there was no randomization. Sample sizes chosen are indicated in the individual figure legends and were not based on formal power calculations to detect pre-specified effect sizes. Data analysis was not blinded.

ACCESSION NUMBERS

The accession numbers for the RNA-seq data reported in this paper are GEO: GSE84878 and GSE88970.

SUPPLEMENTAL INFORMATION

Supplemental Information includes Supplemental Experimental Procedures, seven figures, and six tables and can be found with this article online at http://dx.doi.org/10.1016/j.celrep.2017.04.069.

Figure 7. Downregulation of Essential B Cell Genes in Developmentally Impaired *Whsc1*$^{-/-}$ BM Pro-B Cells

(A) Gene set enrichment analysis (GSEA) plots for the indicated gene sets for the differentially expressed genes in *Whsc1*$^{-/-}$ versus WT BM pro-B cells (see their corresponding heatmaps in Figure S7A). The GSEA comparison was performed (WT minus *Whsc1*$^{-/-}$), so the genes downregulated in the *Whsc1*$^{-/-}$ cells appear at the left of the scale on each graph, and those upregulated appear at the right side. Therefore gene sets downregulated in *Whsc1*$^{-/-}$ cells have a positive normalized enrichment score (NES), and gene sets upregulated in *Whsc1*$^{-/-}$ cells have a negative NES.

(B) GSEA plots for the gene sets corresponding to genes upregulated by either Ebf1 or Pax5 during normal early B cell development (see main text for the generation of the lists of genes). The GSEA analysis shows the global decrease in the levels of expression of these genes in *Whsc1*$^{-/-}$ pro-B cells.

(C) Partial heatmaps corresponding to the GSEA analyses shown in (B). For clarity, only the part corresponding to the genes that become downregulated in *Whsc1*$^{-/-}$ pro-B cells is shown. The full heatmaps can be seen in Figure S7B.

(D) The introduction of a rearranged $V_HD_HJ_H$ B1-8 allele in the *Whsc1*$^{-/-}$ pro-B cells does not rescue the leaky developmental block at the pro-B to pre-B cell transition. The bar graph represents the percentages of the indicated B cell developmental stages in the BM of recipient mice transplanted with cells of the indicated genotypes. n = number of mice analyzed.

See also Figure S7.

AUTHOR CONTRIBUTIONS

E.C.-S. performed the majority of the experiments. M.G. and H.H. generated RNA-seq libraries. E.C.-S., N.D.-S., E.C.-d.-S.-P., A.E.-C., M.D., and C.C. analyzed bioinformatic data. K.U., Y.K., and K.N. provided the *Whsc1*-KO mouse. P.P.R., JH.K., A.A., and J.A.S. designed and performed *IgH* DNA FISH experiments (data not shown). V.D. collaborated in the generation of mouse models (data not shown). C.C. conceived and supervised the project and secured funding. M.L.M.-F. provided conceptual advice. E.C.-S. and C.C. designed the experiments and analyzed and interpreted the data. E.C.-S., M.L.M.-F., and C.C. wrote and edited the manuscript. All authors reviewed the manuscript and provided final approval for submission.

ACKNOWLEDGMENTS

We are indebted to Meinrad Busslinger and Isidro Sanchez-Garcia for useful discussions and for their critical reading of the manuscript. We thank J. Mendez and S. Rodriguez for helpful discussions and help with the DNA fiber analysis; H. Tagoh and M. Fischer for RNA-seq analysis experiments of mature LN B cells; T. Graf, M. Busslinger, A. Rodriguez-Ramiro, and I. Sanchez-Garcia for providing transgenic mouse strains; B. Pintado and the Transgenesis Service of CNB-CBMSO UAM/CSIC for help with the mice; B. Raposo and S. Andrade for FACS sorting; and the Servicio de Microscopía Óptica y Confocal (SMOC) from CBMSO for their help. Research at C.C.'s lab was partially supported by FEDER (Fondo de Investigaciones Sanitarias/Instituto de Salud Carlos III) (PI13/00160 and PI14/00025), Fundación Inocente Inocente, and the ARIMMORA EU/FP7 project and by donations from the Asociación Española del Síndrome de Wolf Hirschhorn (AESWH), the Fundación Síndrome de Wolf-Hirschhorn or 4p- (FSWH4p), FECYT Precipita, and Fundación Ramón Areces. E.C.-S. was partially supported by a JAE-PreDoc fellowship from the Spanish National Research Council (CSIC, FEDER) and was a Residencia de Estudiantes Fellow. N.D.-S. was partially supported by a JAE-intro studentship from the Spanish National Research Council (CSIC) (JAEINT_15_01981). Research at K.U.'s lab was partially supported by the JSTP PRESTO program (4201) and Grants-in-Aid for Scientific Research (22131003 and 15H01345) from MEXT of Japan. P.P.R. is a National Cancer Center and American Society of Hematology Fellow. J.A.S. is a Leukemia & Lymphoma Society (LLS) scholar and NCC and ASH fellow and is supported by NIH grants R01GM086852 and R01GM112192. Research at M.L.M.F.'s lab was partially supported by Instituto de Salud Carlos III and Fundación 1.000 sobre Defectos Congénitos. CIBERER is an initiative of ISCIII, Ministry of Economy and Competitiveness of Spain. V.D. was partially supported by Ministry of Science and Innovation through the Programa tecnicos de apoyo (PTA) from 2012 to 2014. A.E.-C. is funded by the RED-BIO project of the Spanish National Bioinformatics Institute (INB) under grant number PT13/0001/0044. The INB is funded by the Spanish National Health Institute Carlos III (ISCIII) and the Spanish Ministry of Economy and Competitiveness (MINECO). M.D. was funded by the Ministry of Economy and Competitiveness of Spain (PTA2014-09515-I). H.H. is a Miguel Servet (CP14/00229) researcher funded by the Spanish Institute of Health Carlos III (ISCIII). P.P.R. was financed by NIH grant K99GM117302.

Received: November 10, 2016
Revised: February 20, 2017
Accepted: April 24, 2017
Published: May 23, 2017

REFERENCES

Andricovich, J., Kai, Y., Peng, W., Foudi, A., and Tzatsos, A. (2016). Histone demethylase KDM2B regulates lineage commitment in normal and malignant hematopoiesis. J. Clin. Invest. *126*, 905–920.

Battaglia, A., South, S., and Carey, J.C. (2011). Clinical utility gene card for: Wolf-Hirschhorn (4p-) syndrome. Eur. J. Hum. Genet. *19*.

Battaglia, A., Carey, J.C., and South, S.T. (2015). Wolf-Hirschhorn syndrome: a review and update. Am. J. Med. Genet. C. Semin. Med. Genet. *169*, 216–223.

Bergemann, A.D., Cole, F., and Hirschhorn, K. (2005). The etiology of Wolf-Hirschhorn syndrome. Trends Genet. *21*, 188–195.

Chesi, M., Nardini, E., Lim, R.S., Smith, K.D., Kuehl, W.M., and Bergsagel, P.L. (1998). The t(4;14) translocation in myeloma dysregulates both FGFR3 and a novel gene, MMSET, resulting in IgH/MMSET hybrid transcripts. Blood *92*, 3025–3034.

Cobaleda, C., Schebesta, A., Delogu, A., and Busslinger, M. (2007). Pax5: the guardian of B cell identity and function. Nat. Immunol. *8*, 463–470.

Evans, D.L., Zhang, H., Ham, H., Pei, H., Lee, S., Kim, J., Billadeau, D.D., and Lou, Z. (2016). MMSET is dynamically regulated during cell-cycle progression and promotes normal DNA replication. Cell Cycle *15*, 95–105.

Flach, J., Bakker, S.T., Mohrin, M., Conroy, P.C., Pietras, E.M., Reynaud, D., Alvarez, S., Diolaiti, M.E., Ugarte, F., Forsberg, E.C., et al. (2014). Replication stress is a potent driver of functional decline in ageing haematopoietic stem cells. Nature *512*, 198–202.

García-Carpizo, V., Sarmentero, J., Han, B., Graña, O., Ruiz-Llorente, S., Pisano, D.G., Serrano, M., Brooks, H.B., Campbell, R.M., and Barrero, M.J. (2016). NSD2 contributes to oncogenic RAS-driven transcription in lung cancer cells through long-range epigenetic activation. Sci. Rep. *6*, 32952.

Golomb, L., Volarevic, S., and Oren, M. (2014). p53 and ribosome biogenesis stress: the essentials. FEBS Lett. *588*, 2571–2579.

Hajdu, I., Ciccia, A., Lewis, S.M., and Elledge, S.J. (2011). Wolf-Hirschhorn syndrome candidate 1 is involved in the cellular response to DNA damage. Proc. Natl. Acad. Sci. USA *108*, 13130–13134.

Hanley-Lopez, J., Estabrooks, L.L., and Stiehm, R. (1998). Antibody deficiency in Wolf-Hirschhorn syndrome. J. Pediatr. *133*, 141–143.

He, J., Kallin, E.M., Tsukada, Y., and Zhang, Y. (2008). The H3K36 demethylase Jhdm1b/Kdm2b regulates cell proliferation and senescence through p15(Ink4b). Nat. Struct. Mol. Biol. *15*, 1169–1175.

Heng, T.S., and Painter, M.W.; Immunological Genome Project Consortium (2008). The Immunological Genome Project: networks of gene expression in immune cells. Nat. Immunol. *9*, 1091–1094.

Hu, D., and Shilatifard, A. (2016). Epigenetics of hematopoiesis and hematological malignancies. Genes Dev. *30*, 2021–2041.

Huether, R., Dong, L., Chen, X., Wu, G., Parker, M., Wei, L., Ma, J., Edmonson, M.N., Hedlund, E.K., Rusch, M.C., et al. (2014). The landscape of somatic mutations in epigenetic regulators across 1,000 paediatric cancer genomes. Nat. Commun. *5*, 3630.

Jaffe, J.D., Wang, Y., Chan, H.M., Zhang, J., Huether, R., Kryukov, G.V., Bhang, H.E., Taylor, J.E., Hu, M., Englund, N.P., et al. (2013). Global chromatin profiling reveals NSD2 mutations in pediatric acute lymphoblastic leukemia. Nat. Genet. *45*, 1386–1391.

Kais, Z., Rondinelli, B., Holmes, A., O'Leary, C., Kozono, D., D'Andrea, A.D., and Ceccaldi, R. (2016). FANCD2 maintains fork stability in BRCA1/2-deficient tumors and promotes alternative end-joining DNA repair. Cell Rep. *15*, 2488–2499.

Kanu, N., Grönroos, E., Martinez, P., Burrell, R.A., Yi Goh, X., Bartkova, J., Maya-Mendoza, A., Mistrík, M., Rowan, A.J., Patel, H., et al. (2015). SETD2 loss-of-function promotes renal cancer branched evolution through replication stress and impaired DNA repair. Oncogene *34*, 5699–5708.

Kerzendorfer, C., Hannes, F., Colnaghi, R., Abramowicz, I., Carpenter, G., Vermeesch, J.R., and O'Driscoll, M. (2012). Characterizing the functional consequences of haploinsufficiency of NELF-A (WHSC2) and SLBP identifies novel cellular phenotypes in Wolf-Hirschhorn syndrome. Hum. Mol. Genet. *21*, 2181–2193.

Kuo, A.J., Cheung, P., Chen, K., Zee, B.M., Kioi, M., Lauring, J., Xi, Y., Park, B.H., Shi, X., Garcia, B.A., et al. (2011). NSD2 links dimethylation of histone H3 at lysine 36 to oncogenic programming. Mol. Cell *44*, 609–620.

Marango, J., Shimoyama, M., Nishio, H., Meyer, J.A., Min, D.J., Sirulnik, A., Martinez-Martinez, Y., Chesi, M., Bergsagel, P.L., Zhou, M.M., et al. (2008). The MMSET protein is a histone methyltransferase with characteristics of a transcriptional corepressor. Blood *111*, 3145–3154.

Maya-Mendoza, A., Tang, C.W., Pombo, A., and Jackson, D.A. (2009). Mechanisms regulating S phase progression in mammalian cells. Front. Biosci. (Landmark Ed.) *14*, 4199–4213.

Mombaerts, P., Iacomini, J., Johnson, R.S., Herrup, K., Tonegawa, S., and Papaioannou, V.E. (1992). RAG-1-deficient mice have no mature B and T lymphocytes. Cell *68*, 869–877.

Morishita, M., and di Luccio, E. (2011). Cancers and the NSD family of histone lysine methyltransferases. Biochim. Biophys. Acta *1816*, 158–163.

Nimura, K., Ura, K., Shiratori, H., Ikawa, M., Okabe, M., Schwartz, R.J., and Kaneda, Y. (2009). A histone H3 lysine 36 trimethyltransferase links Nkx2-5 to Wolf-Hirschhorn syndrome. Nature *460*, 287–291.

Oyer, J.A., Huang, X., Zheng, Y., Shim, J., Ezponda, T., Carpenter, Z., Allegretta, M., Okot-Kotber, C.I., Patel, J.P., Melnick, A., et al. (2014). Point mutation E1099K in MMSET/NSD2 enhances its methyltranferase activity and leads to altered global chromatin methylation in lymphoid malignancies. Leukemia *28*, 198–201.

Pei, H., Wu, X., Liu, T., Yu, K., Jelinek, D.F., and Lou, Z. (2013). The histone methyltransferase MMSET regulates class switch recombination. J. Immunol. *190*, 756–763.

Pongubala, J.M., Northrup, D.L., Lancki, D.W., Medina, K.L., Treiber, T., Bertolino, E., Thomas, M., Grosschedl, R., Allman, D., and Singh, H. (2008). Transcription factor EBF restricts alternative lineage options and promotes B cell fate commitment independently of Pax5. Nat. Immunol. *9*, 203–215.

Popovic, R., Martinez-Garcia, E., Giannopoulou, E.G., Zhang, Q., Zhang, Q., Ezponda, T., Shah, M.Y., Zheng, Y., Will, C.M., Small, E.C., et al. (2014). Histone methyltransferase MMSET/NSD2 alters EZH2 binding and reprograms the myeloma epigenome through global and focal changes in H3K36 and H3K27 methylation. PLoS Genet. *10*, e1004566.

Revilla-I-Domingo, R., Bilic, I., Vilagos, B., Tagoh, H., Ebert, A., Tamir, I.M., Smeenk, L., Trupke, J., Sommer, A., Jaritz, M., and Busslinger, M. (2012). The B-cell identity factor Pax5 regulates distinct transcriptional programmes in early and late B lymphopoiesis. EMBO J. *31*, 3130–3146.

Sarai, N., Nimura, K., Tamura, T., Kanno, T., Patel, M.C., Heightman, T.D., Ura, K., and Ozato, K. (2013). WHSC1 links transcription elongation to HIRA-mediated histone H3.3 deposition. EMBO J. *32*, 2392–2406.

Shah, M.Y., Martinez-Garcia, E., Phillip, J.M., Chambliss, A.B., Popovic, R., Ezponda, T., Small, E.C., Will, C., Phillip, M.P., Neri, P., et al. (2016). MMSET/WHSC1 enhances DNA damage repair leading to an increase in resistance to chemotherapeutic agents. Oncogene *35*, 5905–5915.

Sonoda, E., Pewzner-Jung, Y., Schwers, S., Taki, S., Jung, S., Eilat, D., and Rajewsky, K. (1997). B cell development under the condition of allelic inclusion. Immunity *6*, 225–233.

Stec, I., Wright, T.J., van Ommen, G.J., de Boer, P.A., van Haeringen, A., Moorman, A.F., Altherr, M.R., and den Dunnen, J.T. (1998). WHSC1, a 90 kb SET domain-containing gene, expressed in early development and homologous to a Drosophila dysmorphy gene maps in the Wolf-Hirschhorn syndrome critical region and is fused to IgH in t(4;14) multiple myeloma. Hum. Mol. Genet. *7*, 1071–1082.

Treiber, T., Mandel, E.M., Pott, S., Györy, I., Firner, S., Liu, E.T., and Grosschedl, R. (2010). Early B cell factor 1 regulates B cell gene networks by activation, repression, and transcription- independent poising of chromatin. Immunity *32*, 714–725.

Ungerbäck, J., Åhsberg, J., Strid, T., Somasundaram, R., and Sigvardsson, M. (2015). Combined heterozygous loss of Ebf1 and Pax5 allows for T-lineage conversion of B cell progenitors. J. Exp. Med. *212*, 1109–1123.

Wagner, E.J., and Carpenter, P.B. (2012). Understanding the language of Lys36 methylation at histone H3. Nat. Rev. Mol. Cell Biol. *13*, 115–126.